NACA RM E58C04

NACA

RESEARCH MEMORANDUM

ANALYSIS OF TRANSONIC ROTOR-BLADE PASSAGE LOSS WITH HOT-WIRE ANEMOMETERS

By George W. Lewis, Edward R. Tysl, and Theodore E. Fessler

Lewis Flight Propulsion Laboratory
Cleveland, Ohio

NATIONAL ADVISORY COMMITTEE
FOR AERONAUTICS

WASHINGTON
June 5, 1958
Declassified March 18, 1960

NATIONAL ADVISORY COMMITTEE FOR AERONAUTICS

RESEARCH MEMORANDUM

4368

CS-1

ANALYSIS OF TRANSONIC ROTOR-BLADE PASSAGE LOSS WITH HOT-WIRE ANEMOMETERS

By George W. Lewis, Edward R. Tysl, and Theodore E. Fessler

SUMMARY

Experimental data are analyzed to support present theory associated with total-pressure loss in the supersonic flow regions of transonic compressor rotors. At compressor minimum-loss operation blade-to-blade loss distributions as obtained by means of a hot-wire anemometer and as calculated from shock-loss considerations are presented. Data are obtained for the rotor operating at three tip speeds (inlet relative Mach numbers of 1.06, 1.17, and 1.26) and three levels of tip element solidity (0.97, 0.83, and 0.69). Both shock and blade profile losses increase with increasing tip speed. As solidity decreases, the intersection of the passage shock with the blade suction surface moves further downstream resulting in increased blade surface Mach numbers and, consequently, increased loss.

INTRODUCTION

Transonic compressors provide high stage pressure ratios and high mass flows that can be useful in achieving light weight turbojet compressor units. To fulfill the requirements of these units, the efficiency of the transonic compressor must be comparable with the efficiency of the subsonic compressor unit. Adequate performance has been achieved by transonic compressor rotors operating at blade relative inlet Mach numbers up to 1.1. In higher Mach number designs, however, rotors were not producing the design conditions of weight flow and efficiency. In order to improve performance at the higher Mach numbers, information of the loss phenomena must be obtained.

Reference 1 presents some ideas on the type of flow field that may exist in a transonic axial-flow compressor and endeavors to establish a simple model that may be used to estimate losses occurring in high Mach number flow regimes. The analysis assumes that the losses originating in the supersonic elements of the transonic compressor rotor

could be divided into two main factors: (1) the shock-wave losses, which result in total-pressure loss in the free stream between blades, and (2) the profile losses which are due to viscous flow effects on the blade surfaces and result in blade wakes. The model developed in that investigation was used to explain variations of blade-element loss with, among other things, changes in inlet relative Mach number and rotor solidity.

This report presents data from measurements of the flow in a single-stage research compressor, which supports the model of reference 1. The research rotor was operated at three speeds and three levels of solidity. Rotor-outlet flow measurements were made under these conditions by means of both temperature- and pressure-measuring probes and by a hot-wire anemometer capable of resolving the blade-to-blade flow pattern. A calculated shock technique similar to that of reference 1 is incorporated with these experimental results. Another approach for estimating passage shock loss given a flow rate and blade geometry was reported in reference 2.

APPARATUS

The variable-component test rig discussed in reference 3 was used for this investigation. A schematic diagram of the test facility is shown in figure 1. Room air was measured by a submerged thin plate orifice and filtered by an electrostatic-mechanical filter before entering a large entrance tank. The air was then accelerated through a smooth bellmouth to the test section and discharged to a large collector leading to the laboratory altitude exhaust system. The compressor rotor was cantilever mounted on a two-bearing shaft arrangement and was driven through a speed-increasing gear box by a variable frequency induction motor.

Compressor Rotor

The research transonic compressor rotor had a tip diameter of 20 inches at the inlet that decreased to 19.2 inches at the outlet. The hub diameter for this configuration was constant at 12 inches.

The blades (ref. 3) for this compressor rotor were made up of double circular-arc sections and stacked radially so that the trailing edge of each rotor blade lies in a plane normal to the axis of rotation.

Instrumentation

Instrument survey stations were established at the axial locations indicated in figure 1. (All stations and symbols are defined in

appendix A). The investigation required the use of the usual compressor instrumentation (ref. 4) plus a hot-wire anemometer, which would be sensitive to blade wakes and other flow fluctuations.

The compressor rotor was tested using two sets of instrumentation downstream of the rotor. Blade-element data and over-all performance were taken from the usual survey probes of reference 3. Hot-wire probes replaced the survey probes at station 2 of figure 1 and total-pressure and temperature rakes were placed at station 3.

A hot-wire anemometer was located 1/4 inch downstream of the rotor-blade trailing edge. The hot-wire probe had a 0.0002-inch-diameter tungsten wire with an effective length of 0.040 inch. The axis of the wire was perpendicular to a radial line normal to the axis of rotation and normal to the compressor-rotor axial-flow direction. Thus, the wire was sensitive to changes in the axial component of mass flow. The radial flow component was assumed to be negligible. This orientation was selected because the axial component of the flow relative to the rotor blade row can be measured directly, thus facilitating the calculation of a blade-element loss. The hot-wire anemometer was a constant-temperature type and had a frequency response of at least 40,000 cps. Rotor-blade frequency encountered in this investigation varied from 2900 to 4800 blades per second. Because of the small physical dimensions of the wire as compared to the blade spacing and the high frequency response of the system, the definition of blade wakes was good.

Methods and Procedure

The data presented in this report were obtained at rotor-inlet corrected tip speeds of 1000, 1100, and 1200 feet per second. The rotor was tested with 21, 18, and 15 blades, resulting in a solidity variation at the element 10 percent of passage height from the tip (hereafter referred to as tip element) of 0.97, 0.83, and 0.69. In this transonic rotor-blade investigation, no guide vanes or stator blades were used.

The compressor-rotor over-all performance parameters were computed by mass averaging of pressure, temperature, and angle data obtained from surveys at the rotor outlet. The weight flow was computed from measurements taken from a submerged thin plate orifice. Blade-element performance was computed from the survey data and methods given in reference 4.

Hot-wire traces photographed from an oscilloscope screen were used to indicate the distribution of loss. The method of computing loss from these traces is the same as that indicated in reference 3 with one exception. Reference 3 assumes zero loss at the lowest part of the hot-wire trace while this method assumes a minimum free-stream shock loss as presented in appendix B of this report.

ANALYSIS

The flow model set forth in reference 1 is two-dimensional, and, in that respect, similar to the blade-element approach usually employed in compressor studies (ref. 5). This type of model rules out consideration of the flow phenomena in the blade-tip flow (ref. 3) as well as the three-dimensional effects of the mixed subsonic and supersonic flow fields in a transonic compressor. The two-dimensional flow hypothesis, however, greatly simplifies the analysis and allows the comparison of transonic blade-element data with subsonic compressor and cascade data. It is thus important to test this hypothesis by comparison with experiment.

Description of Flow Model

According to the analysis of reference 1, the shock-wave configuration in the supersonic elements of a transonic compressor rotor is like that shown in figure 2(a) and similar to the flow model of reference 1. On the basis of this shock-wave configuration, a circumferential variation of relative total pressure downstream of a rotor-blade element is deduced for the case of a supersonic inlet Mach number. The loss in total-pressure, relative to the blades, caused by the passage shock is shown schematically in figure 2(b) while the combined effects of blade passage shock and blade profile losses (due to viscous effects and shock-wave - boundary-layer interaction effects) on total-pressure loss are shown schematically in figure 2(c).

Several effects are important in determining the strength of the shock wave and, consequently, the total-pressure loss, due to the shock wave standing in the blade passage. The strength of the shock wave (as measured by the upstream Mach number) is principally determined by the level of the blade-inlet relative Mach number and by the amount of supersonic turning the airstream undergoes in passing over the suction surface of the blade. Unfortunately, the previously mentioned flow model is not yet useful in establishing the exact location of the shock wave in the blade passage. Consequently, the distribution of total-pressure loss due to this shock wave cannot as yet be predicted with any degree of certainty.

To obtain some estimate of these losses, however, an arbitrary placement of the shock wave was devised in reference 1 and is shown in figure 3 as line gf". Reference 1 assumes that the passage shock loss can be approximated by the normal shock loss for a Mach number that is an average of the values occurring at points g and f". The information necessary for the calculation is the inlet relative Mach number M_1' (assumed to occur at point g), the inlet relative air direction β_1', and the point f" at which the passage shock wave intersects the

suction surface. With point f" known and the flow direction at this point assumed to be tangent to the blade suction surface, the Mach number at this point can be calculated (assuming two-dimensional isentropic flow). A procedure for obtaining the point f" on the blade surface is detailed in appendix B of reference 1 for double circular-arc-type airfoils.

Experimental Verification

To provide experimental evidence in support of the flow model already described, the compressor test facility and instrumentation of reference 3 were used to obtain blade passage loss distributions at transonic speeds. Measurements of the rotor-outlet flow by means of the hot-wire anemometer, together with time-averaged pressure and temperature measurements, were used to determine the actual blade-to-blade variations of total-pressure loss coefficient at minimum loss incidence angle. These loss distributions were similar to those predicted in reference 1, that is, there was evidence of the predicted combination of shock-wave, viscous, and shock - boundary-layer interaction losses.

Treatment of Hot-Wire Data

The hot-wire signals were observed and recorded as displayed on an oscilloscope screen. These data (representing the flow variations at the tip element station of the compressor rotor) were taken at performance levels indicated as solid symbols in figures 4 and 5. These performance data (solid symbols that differ from the open-symbol data computed from station 2 measurements) were computed from measurements from total-pressure and temperature rakes located at station 3 of figure 1. Actual photographs of the hot-wire signals displayed on the oscilloscope are shown in figures 6(a) and (b). The two peak points in each photograph represent the blade wakes as described in detail in reference 3.

A passage loss distribution computed from a hot-wire trace using the technique of reference 3 is shown in figure 7. The high-loss regions near the blade suction and pressure surfaces are due to viscous effects. This type of loss was reported in reference 3. In the free-stream portion of the blade passage the losses increase from the blade pressure to the blade suction surface. Reference 1 discusses this free-stream loss trend in a flow model and attributes it to passage shock and shock - boundary-layer interaction. In order to assign a magnitude to this free-stream loss, the level of the hot-wire loss was raised until the integrated mass-averaged value was comparable to the measured time-averaged loss. The method raising this hot-wire loss is presented in appendix B. The results of this treatment of the hot-wire data are believed to be a

good representation of the actual total-pressure loss variations across the blade passage. This variation, then, is to be compared with the calculated shock-loss variation by a method similar to reference 1.

Shock-Wave Configurations

Initial passage shock losses were calculated by assuming that the passage shock wave lies on line ff" of figure 3 and integrating the loss at a number of points along this line. Comparisons with the hot-wire data indicated that the calculated values of shock loss were considerably higher than those measured. Theoretical considerations as well as some preliminary data from fast-response pressure probes (to be reported) indicated that this disagreement should have been expected. The cause of the disagreement lays in the arbitrary placement of the passage shock wave used to obtain the calculated loss variation.

A new shock-wave position was determined and found by the following procedure. A midpassage location of the shock wave was found that would give a calculated midpassage pressure loss equal to that measured by the hot wire (maintaining the two-dimensional flow assumption), and the orientation of the wave was arbitrarily moved forward but remained parallel to that used previously. The shock-wave movement was found to agree quite well with theoretical estimates and independent data, references 6 and 7. Hence, this procedure was adopted as standard treatment for the comparisons presented in the following section. (All data and calculations are for minimum loss incidence-angle operation.)

Predicted Trends

The rotor operating conditions and configurations tested in this investigation were selected to point out two important factors determining shock losses in transonic machines, namely, inlet Mach number level and rotor blade solidity. For the types of transonic compressors generally designed, the inlet relative Mach number is restricted to a narrow range of perhaps 1.0 to 1.3. These Mach numbers are, in themselves, quite inoffensive. There is, however, a pronounced effect in terms of total-pressure loss due to slight changes in inlet Mach number. The cause of this strong dependency lies in the sensitivity of peak suction surface Mach number on blade inlet Mach number. Reference 1 shows that these suction surface Mach numbers often reach values as high as 1.7 for which the computed shock-loss coefficient (no profile loss) may exceed 0.1. Thus, a serious increase in blade element shock losses may be caused by a relatively small increase in rotor-inlet relative Mach number.

The effect of rotor solidity on supersonic turning is clearly shown in figure 5 of reference 1. As solidity is decreased the intersection of the blade passage shock wave and the blade suction surface moves farther back along the blade resulting in an increase in the peak suction surface Mach number and, consequently, the high shock-loss coefficient and shock - boundary-layer interactions. Thus, for a given design, increasing losses are expected to accompany decreasing solidity in the transonic regime.

EXPERIMENTAL RESULTS

Rotor performance for the three speed and solidity levels tested in this investigation are shown in the over-all and blade-element performance maps of figures 4 and 5. These data are presented only to provide an indication of the level of rotor performance investigated.

Figure 8 shows the measured and calculated variations of total-pressure-loss coefficient across the blade passages for three tip speeds (inlet relative Mach numbers) at a fixed solidity of 0.83 (symbols represent the measured hot-wire loss variation). For general interest the location of the calculated shock wave in leading-edge diameters ahead of the blade leading edge is also given in figure 8. However, at this time no attempt is made to correlate these data. The effect of increasing rotor-inlet Mach number is clear from these results. Except for that portion of the passage near the blade surfaces, the variations of measured- and calculated-loss variation are very similar. The cause for the difference of the two curves in the blade surface regions is a combination of viscous effects and a lambda shock configuration. This condition is discussed in reference 1.

The effects of solidity variations on blade passage loss are shown in figure 9 where the calculated- and measured-loss variations are very similar except near the blade suction surfaces. This increase in over-all loss as solidity decreases is primarily due to the increased loss near the blade suction surface.

CONCLUDING REMARKS

The results presented herein provide experimental evidence of the blade-to-blade (circumferential) variation of total-pressure loss for a blade element operating at typical transonic inlet relative Mach numbers. These data give evidence of the type of flow predicted in reference 1 and further indicate the need of a flow model such as that suggested in reference 1 for the analysis and prediction of total-pressure losses due to a passage shock.

The results of experimental data reflect the influence of the blade peak suction-surface Mach number on loss levels in transonic flow. The effects of two design parameters, inlet relative Mach number and blade solidity, are shown.

4368

Lewis Flight Propulsion Laboratory
National Advisory Committee for Aeronautics
Cleveland, Ohio, March 13, 1958

APPENDIX A

SYMBOLS

A_f frontal area

a speed of sound

c' blade chord, less leading- and trailing-edge radii, in.

D diffusion factor

i incidence angle, angle between inlet-air direction and tangent to blade mean camber line at leading edge, deg

M Mach number

P total pressure, lb/sq ft

p static pressure, lb/sq ft

r_{le} blade-leading-edge radius

r_s radius of curvature of blade suction surface

U_t rotor tip speed, ft/sec

V air velocity, ft/sec

w weight flow, lb/sec

x coordinate system (fig. 10)

y coordinate system (fig. 10)

α slope of shock with coordinate system, deg

β_1 air angle, angle between air velocity and axial direction, deg

γ ratio of specific heats

γ^o blade-chord angle, angle between blade chord and axial direction, deg

δ ratio of inlet total pressure to NACA standard sea-level pressure of 2116 lb/sq ft

δ^o angle of tangent to blade surface with the chord line at point n, deg

η_t adiabatic temperature-rise efficiency

θ ratio of total temperature to NACA standard sea-level temperature of 518.7° F

$\varkappa$ blade angle, angle between tangent to blade mean camber line and axial direction, deg

μ Mach angle, angle of expansion line with the tangent to the blade surface at point n, deg

ν Prandtl-Meyer expansion angle (ref. 8)

ξ angle used in fig. 10, deg

ρ static density of air, lb/cu ft

Σ angle used in fig. 10, deg

σ' solidity, ratio of blade chord (c') to spacing

φ camber angle, $\varkappa_1 - \varkappa_2$, deg

$\overline{\omega}$ total-pressure-loss coefficient

$\overline{\omega}_s$ computed shock-loss coefficient

Subscripts:

a upstream of passage shock

b downstream of passage shock

f shock reference, fig. 10

g shock reference, fig. 10

i intercept of expansion line with shock

id ideal

m.a. mass averaged

n point on blade suction surface

s suction surface

z axial component

0 stagnation condition

1 rotor inlet

2 rotor outlet

Superscripts:

' relative to rotor

" shock contact on blade surface

APPENDIX B

CALCULATION OF BLADE PASSAGE LOSSES

In the analysis of the loss data presented, two operations were necessary: (1) to elevate the passage hot-wire trace to a level where the hot-wire mass-average integrated loss approximated time-average measured loss, and (2) to gain a better correlation of computed shock loss with the hot-wire distribution by moving the passage shock forward of the blade leading edge.

Hot-Wire Trace

A procedure for transferring the hot-wire trace data to total-pressure-loss data is presented in appendix B of reference 3. An inclusion of a pressure recovery term for flow across a shock is incorporated as follows:

Assume an average pressure recovery across the passage shock P'_b/P'_a, then from the table of reference 8 obtain a new Mach number behind the shock M'_b:

Obtain a new $P'_2/P'_{2,id}$ from the curves of equation (B9) of reference 2.

$$\frac{\rho V_z}{(\rho V_z)_{id}} = \left(\frac{P'_2}{P'_{2,id}}\right)^{\frac{\gamma-1}{\gamma}} \left[\frac{1 - \left(\frac{p}{P'}\right)_b^{\frac{\gamma-1}{\gamma}}}{1 - \left(\frac{p}{P'}\right)_{id}^{\frac{\gamma-1}{\gamma}}}\right]^{1/2}$$

by using the new M'_b and the computed $\rho V_z/(\rho V_z)_{id}$ from the hot-wire trace.

The final step is to include the initial shock recovery with the computed hot-wire recovery.

$$\frac{P'_2}{P'_{2,id}} \times \frac{P'_b}{P'_a} = \frac{P'_2}{P'_a}$$

where

$$P'_{2,id} = P'_b$$

This new pressure ratio is then used to compute the relative total-pressure loss

$$\overline{\omega} = \frac{1 - \frac{P'_2}{P'_a}}{1 - \left(\frac{p}{P'}\right)_{M'_1}}$$

Shock-Loss Calculation

The particular blade geometry concerned with locating a passage shock line in the upstream flow field (circular-arc blades) is shown in figure 10. The method and procedure for locating the shock line ff" were presented in appendix B of reference 1. The new location of the passage shock line gg" is moved forward a distance Δx into a lower supersonic flow field. The flow area into the blade passage is reduced Δy distance to approximate a stagnation streamline to the next adjoining blade. Intersection of supersonic expansion lines from the blade suction surface with the assumed shock gg" sets up the flow field for computing the mass-averaged shock losses using the blade geometry as follows:

(1) Determine the coordinates of the points f and f"

$$y_f = \frac{c' \cos \gamma^o}{\sigma'}$$

$$x_f = \frac{y_f}{\cot \gamma^o} - r_{le}$$

$$\Sigma = \tan^{-1}\left(\frac{\sin \varkappa_1 \sin \frac{\varphi}{2}}{\sigma' + \cos \varkappa \sin \frac{\varphi}{2}}\right) \text{ (from ref. 1)}$$

$$x_{f''} = \frac{c'}{2}\left(1 + \sin 2\Sigma_1 \cot \frac{\varphi}{2} - \cos 2\Sigma\right)$$

$$\xi_{f''} = \sin^{-1}\left[\sin\frac{\varphi_s}{2}\left(\frac{x_{f''}}{\frac{c'}{2}} - 1\right)\right]$$

$$y_{f''} = r_s \cos\xi_{f''} - \left(r_s \cos\frac{\varphi_s}{2} - r_{le}\right)$$

(2) Find the slope of ff"

$$\alpha = \tan^{-1}\left(\frac{y_f - y_{f''}}{x_f - x_{f''}}\right)$$

(3) Locate x_g and $x_{g''}$ by selecting Δx

$$x_f - \Delta x = x_g$$

$$x_{f''} - \Delta x = x_{g''}$$

(4) Find $\xi_{g''}$ from

$$\xi_{g''} = \sin^{-1}\left[\sin\frac{\varphi_s}{2}\left(\frac{x_{g''}}{\frac{c'}{2}} - 1\right)\right]$$

(5) Locate $y_{g''}$

$$y_{g''} = r_s \cos\xi_{f''} - \left(r_s \cos\frac{\varphi_s}{2} - r_{le}\right)$$

(6) Find the y intercept b"

$$b'' = y_{g''} - x_{g''} \tan\alpha$$

(7) Solve for y_g (assumed stream-tube reduction)

$$y_g = y_f - \Delta x \tan\frac{\varphi}{2}$$

(8) Get the blade suction-surface inlet conditions

$$\varkappa_s = \gamma^o + \frac{\varphi_s}{2}$$

4368

Locate n points on the blade suction surface at equal degree increments in the x-y coordinate system. The leading-edge angle with respect to the x-axis is $(\varphi/2)_{n=0}$ at $n = 1$; $\delta^{o}_{n=1} = \varphi_s/2 - 1$.

Set up inlet conditions given the inlet flow direction and relative Mach number.

Subtract blade suction-surface angle $\varkappa_s$ from flow direction β'_1 to compute the leading-edge turning. If the turning is positive, add to the initial expansion from M'_1. If the turning is negative (compression waves), locate the point n on the blade suction surface where the flow is accelerated back to ν of M'_1.

Compute the expansion line from point n on the blade suction surface that intersects the shock line near y_g.

(1) From ν_n obtain M'_n and μ_n

$$\tan (\delta^{o}_{n} + \mu_n) \text{ (Mach angle with respect to } x\text{-axis)}$$

$$y_n - x_n \tan (\delta^{o}_{n} + \mu_n) = b_n \text{ (intercept with } y\text{-axis)}$$

$$\frac{b_n \tan \alpha - b'' \tan (\delta^{o}_{n} + \mu_n)}{\tan \alpha - \tan (\delta^{o}_{n} + \mu_n)} = y_i$$

(2) Compute the y-intercept for each expansion line across the passage shock and obtain the normal (to the shock) component of this Mach number.

(3) From the Ames tables (ref. 8) and normal component of the Mach number obtain

$$P'_b/P'_a$$

(4) Compute then the loss at the point on the shock line

$$\bar{\omega}_s = \frac{1 - \frac{P'_b}{P'_a}}{1 - \left(\frac{p}{P}\right)_{M'_1}}$$

(5) Plot $\bar{\omega}_s$ against passage height $\left(\frac{y_i - y_{g''}}{y_g - y_{g''}}\right)$

(6) From M'_n for each expansion wave obtain from Ames tables ρ/ρ_0 and a/a_0.

(7) Obtain weight-flow parameter $\left[M'_n \sin(\alpha - \delta^o) \frac{\rho}{\rho_0} \frac{a}{a_0}\right]_n$

$$(8) \quad \frac{\int_{y_{g''}}^{y_g} M'_n \sin(\alpha - \delta^o) \frac{\rho}{\rho_0} \frac{a}{a_0} \frac{P'_b}{P'_a} dy}{\int_{y_{g''}}^{y_g} M'_n \sin(\alpha - \delta^o) \frac{\rho}{\rho_0} \frac{a}{a_0} dy} = \left(\frac{P'_b}{P'_a}\right)_{m.a.}$$

$$(9) \quad (\bar{\omega}_s)_{m.a.} = \frac{1 - \left(\frac{P'_b}{P'_a}\right)_{m.a.}}{1 - \left(\frac{p}{P'}\right)_{M'_1}} \text{ (average shock loss)}$$

REFERENCES

1. Schwenk, Francis C., Lewis, George W., and Hartmann, Melvin J.: A Preliminary Analysis of the Magnitude of Shock Losses in Transonic Compressors. NACA RM E57A30, 1957.

2. Miller, Genevieve R., and Hartmann, Melvin J.: Experimental Shock Configurations and Shock Losses in a Transonic-Compressor Rotor at Design Speed. NACA RM E58A14b, 1958.

3. Fessler, Theodore E., and Hartmann, Melvin J.: Preliminary Survey of Compressor Rotor-Blade Wakes and Other Flow Phenomena with a Hot-Wire Anemometer. NACA RM E56A13, 1956.

4. Schwenk, Francis C., Lieblein, Seymour, and Lewis, George W.: Experimental Investigation of an Axial-Flow Compressor Inlet Stage Operating at Transonic Relative Inlet Mach Numbers. III - Blade-Row Performance of Stage with Transonic Rotor and Subsonic Stator at Corrected Tip Speeds of 800 and 1000 Feet per Second. NACA RM E53G17, 1953.

4368

5. Lieblein, Seymour: Review of High-Performance Axial-Flow-Compressor Blade-Element Theory. NACA RM E53L22, 1954.

6. Klapproth, John F.: Approximate Relative-Total-Pressure Losses of an Infinite Cascade of Supersonic Blades with Finite Leading-Edge Thickness. NACA RM E9L21, 1950.

7. Moeckel, W. E.: Approximate Method for Predicting Form and Location of Detached Shock Waves Ahead of Plane or Axially Symmetrical Bodies. NACA TN 1921, 1949.

8. Ames Research Staff: Equations, Tables, and Charts for Compressible Flow. NACA Rep. 1135, 1953. (Supersedes NACA TN 1428.)

4368

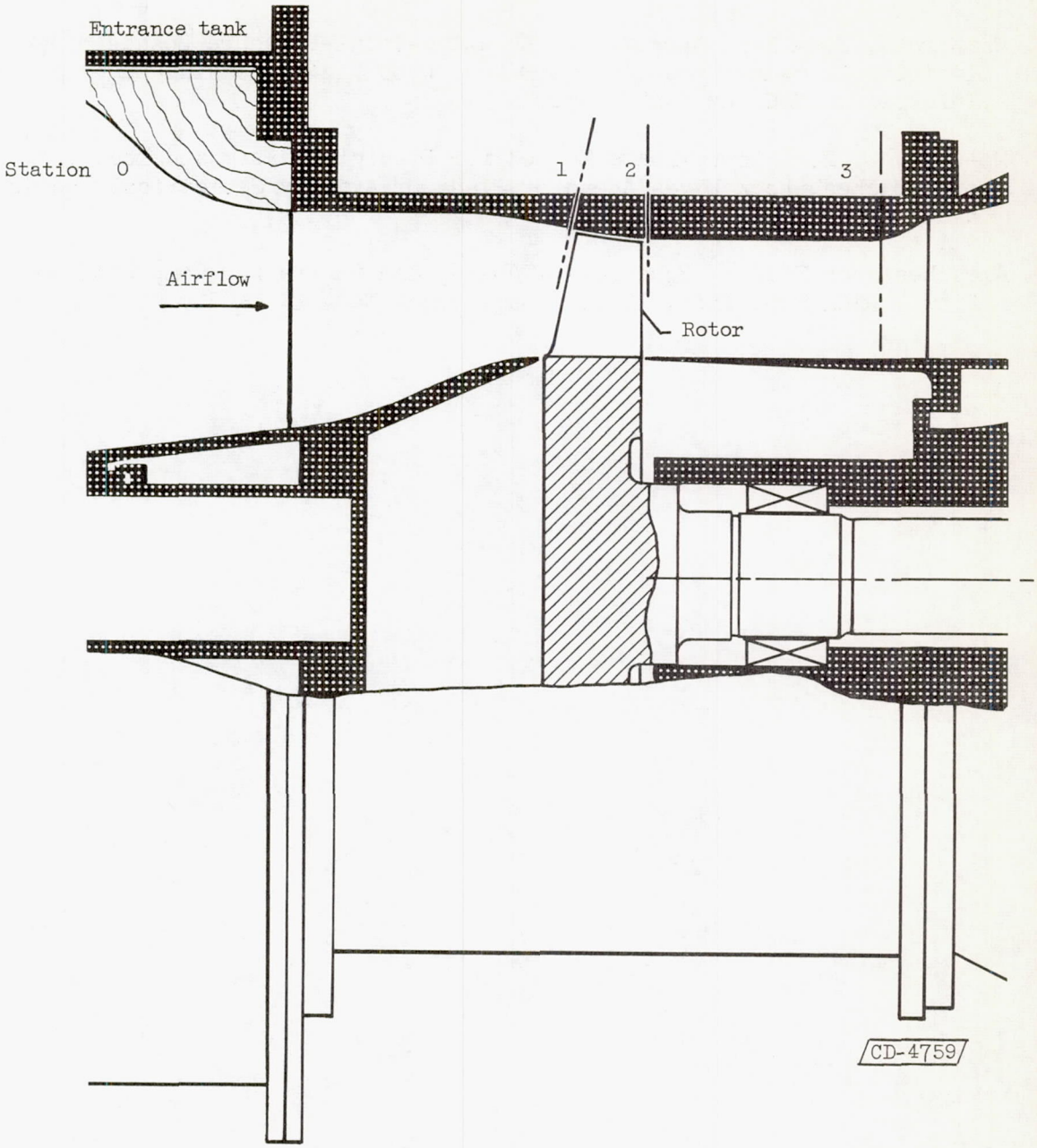


Figure 1. - Schematic view of compressor test section showing location of instrument stations.

4368
CS-3 back

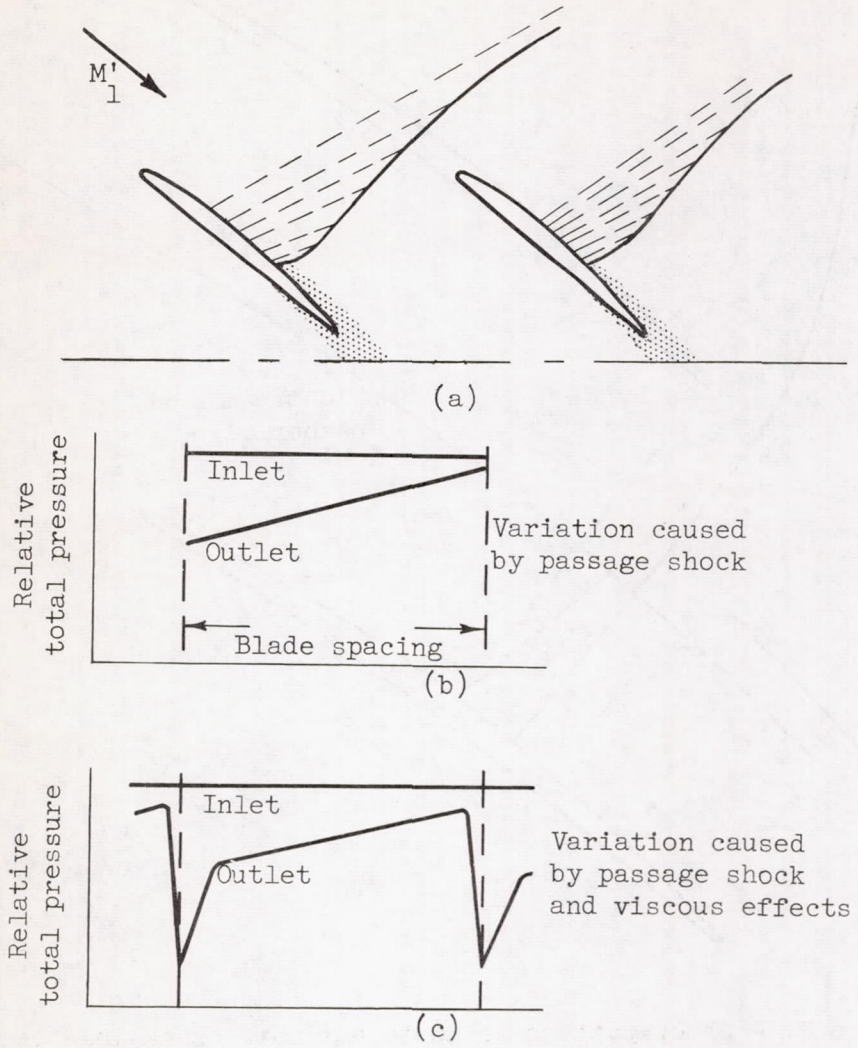


Figure 2. - Circumferential (blade-to-blade) variation of relative total pressure.

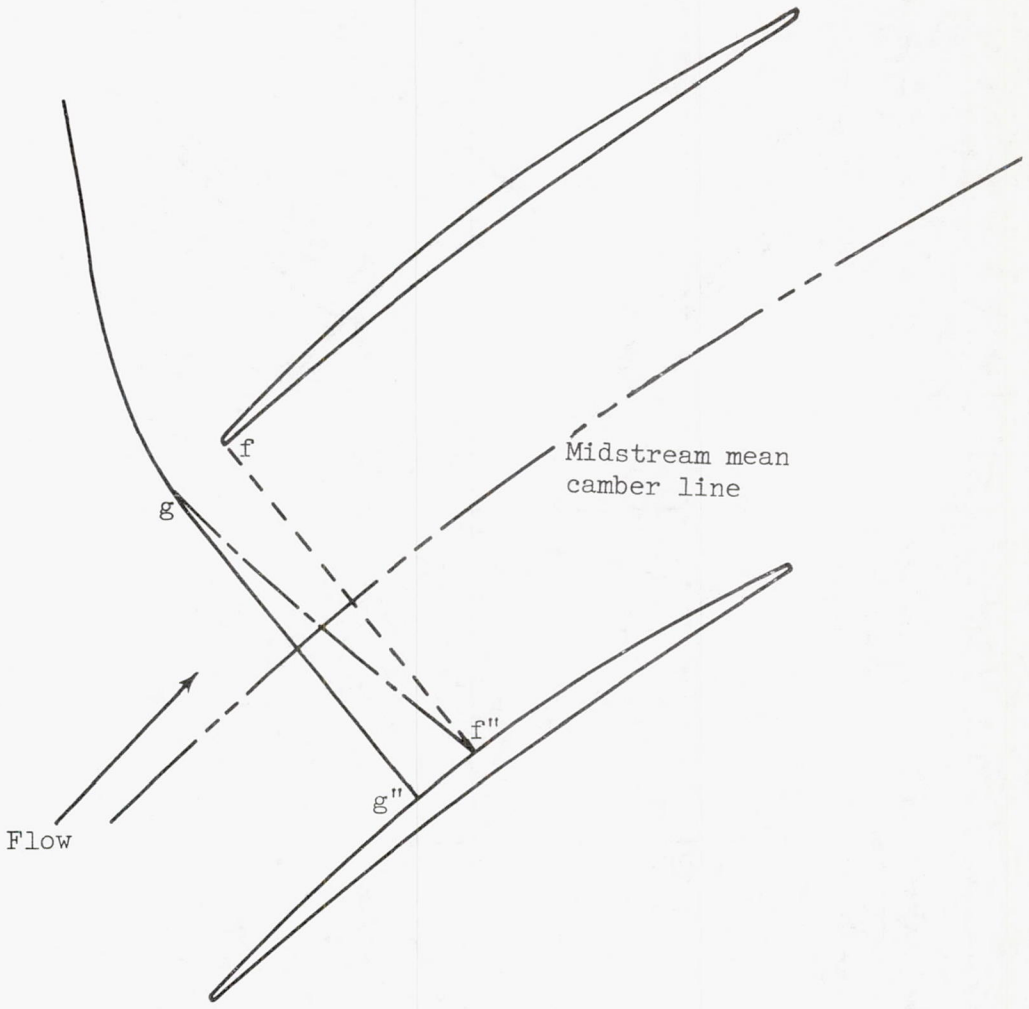
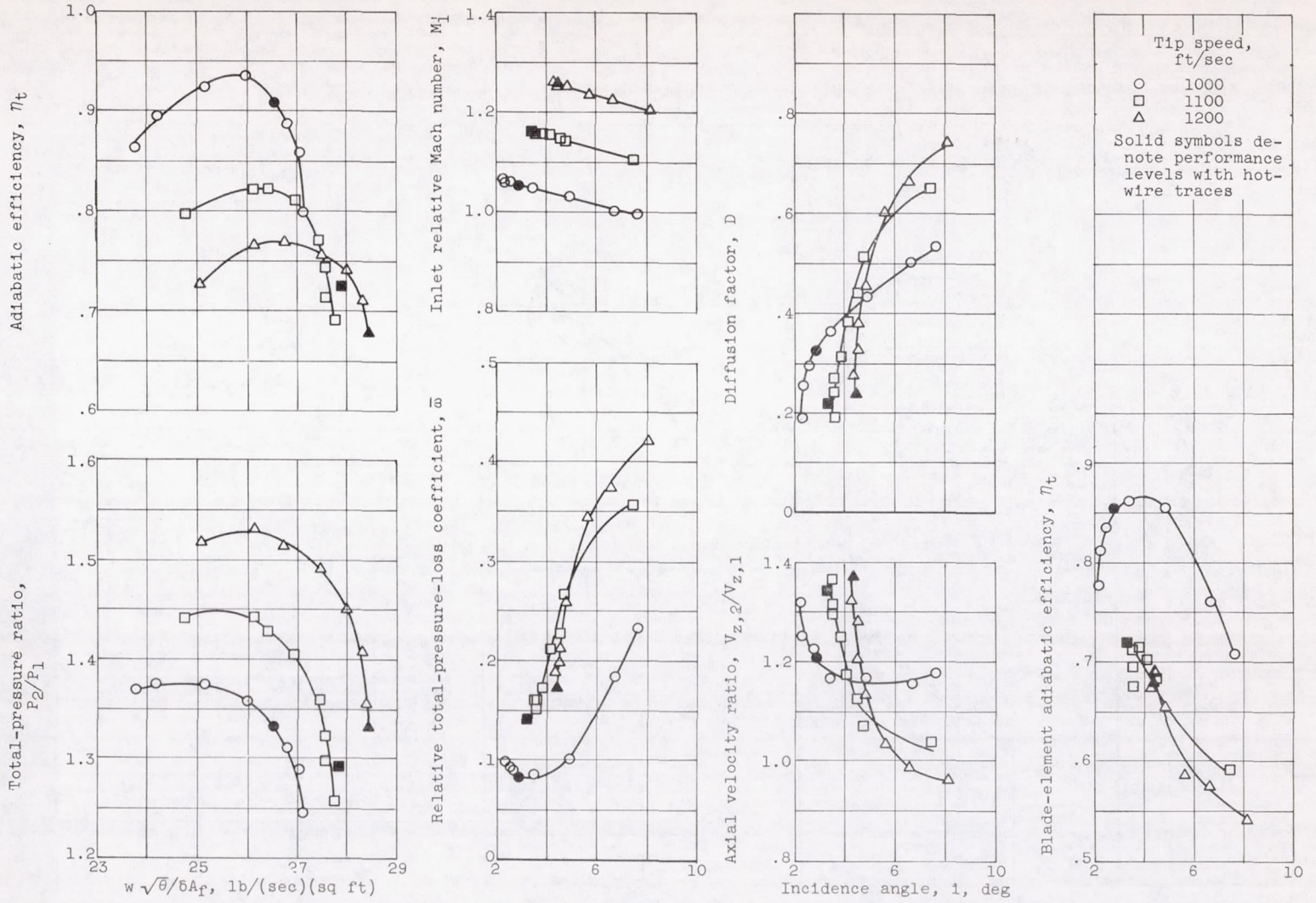


Figure 3. - Shock-pattern setup to estimate shock-loss levels.



(a) Over-all performance.

(b) Blade-element (tip) performance.

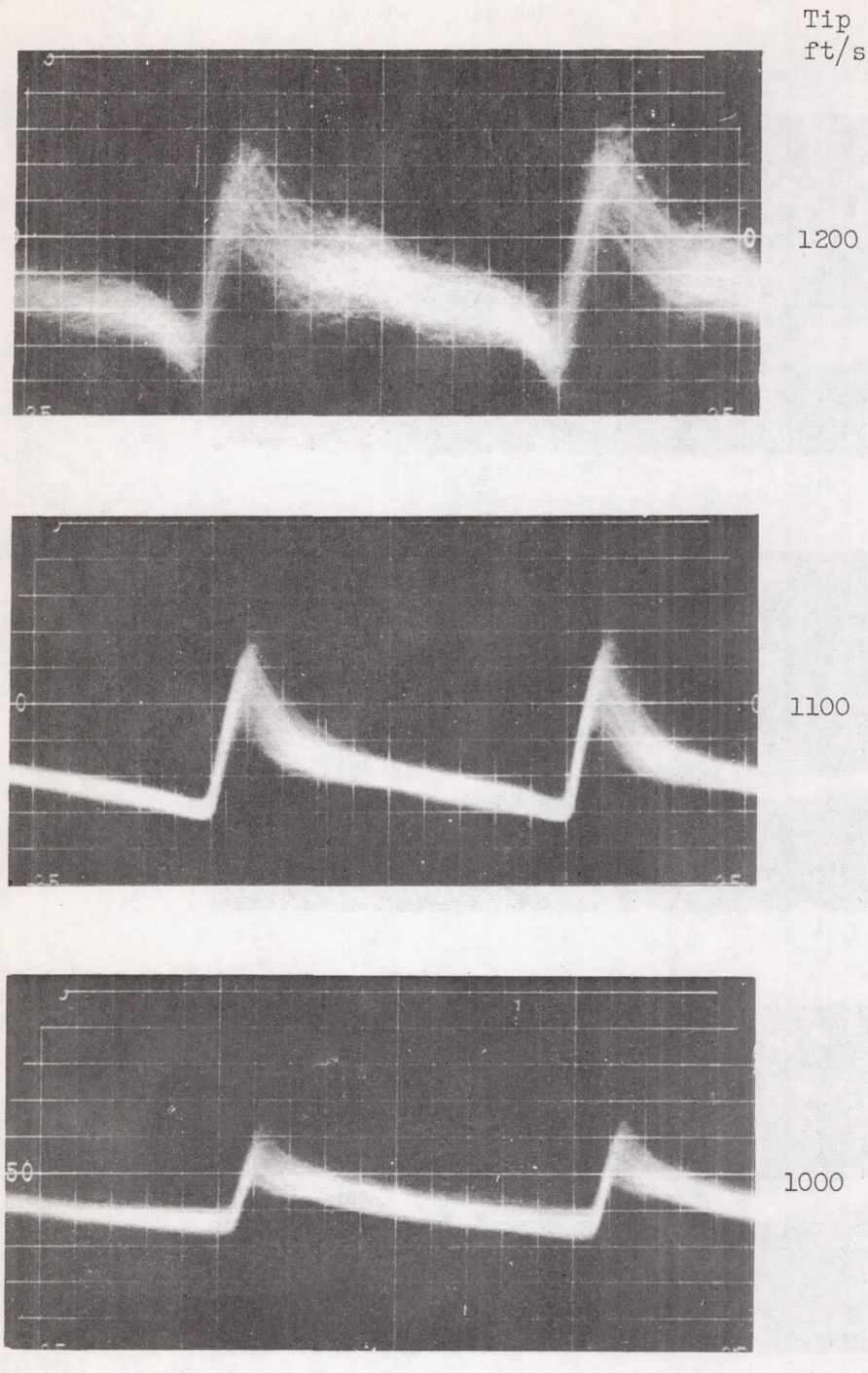
Figure 4. - Over-all and blade-element (tip section) performance of the 20-inch-diameter research compressor rotor having a solidity of 0.83.

(a) Over-all performance.

(b) Blade element (tip) performance

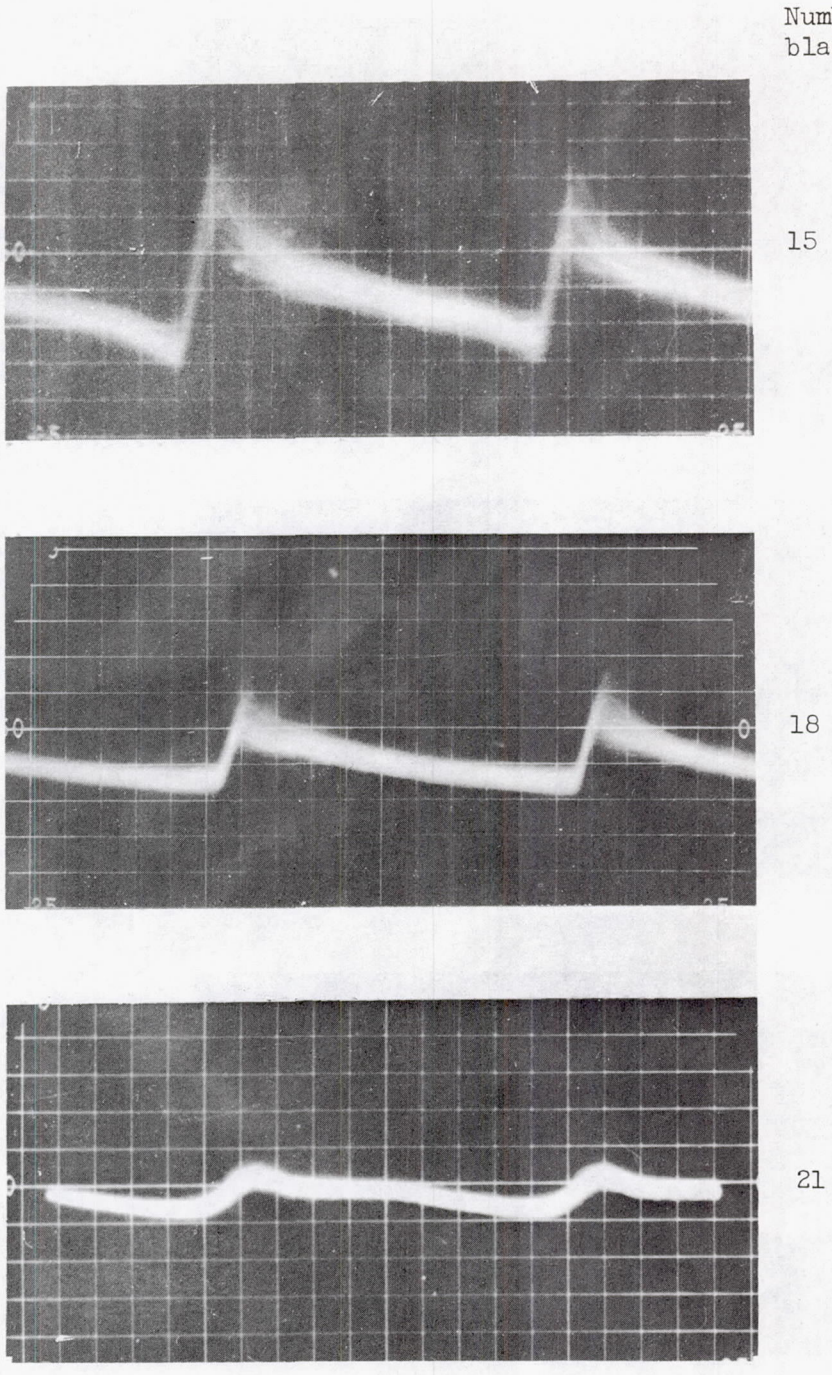
Figure 5. - Over-all and blade-element (tip) performance of three solidities of the 20-inch-diameter research compressor rotor.

4368



(a) Flow pattern at a tip solidity of 0.83 and at three levels of tip speed.

Figure 6. - Photographs of hot-wire anemometer traces showing compressor-rotor blade-to-blade flow distribution at the blade tip element.



(b) Flow pattern at a tip speed of 1000 feet per second and at three solidities.

Figure 6. - Photographs of hot-wire anemometer traces showing compressor-rotor blade-to-blade flow distribution at the blade tip element.

4368

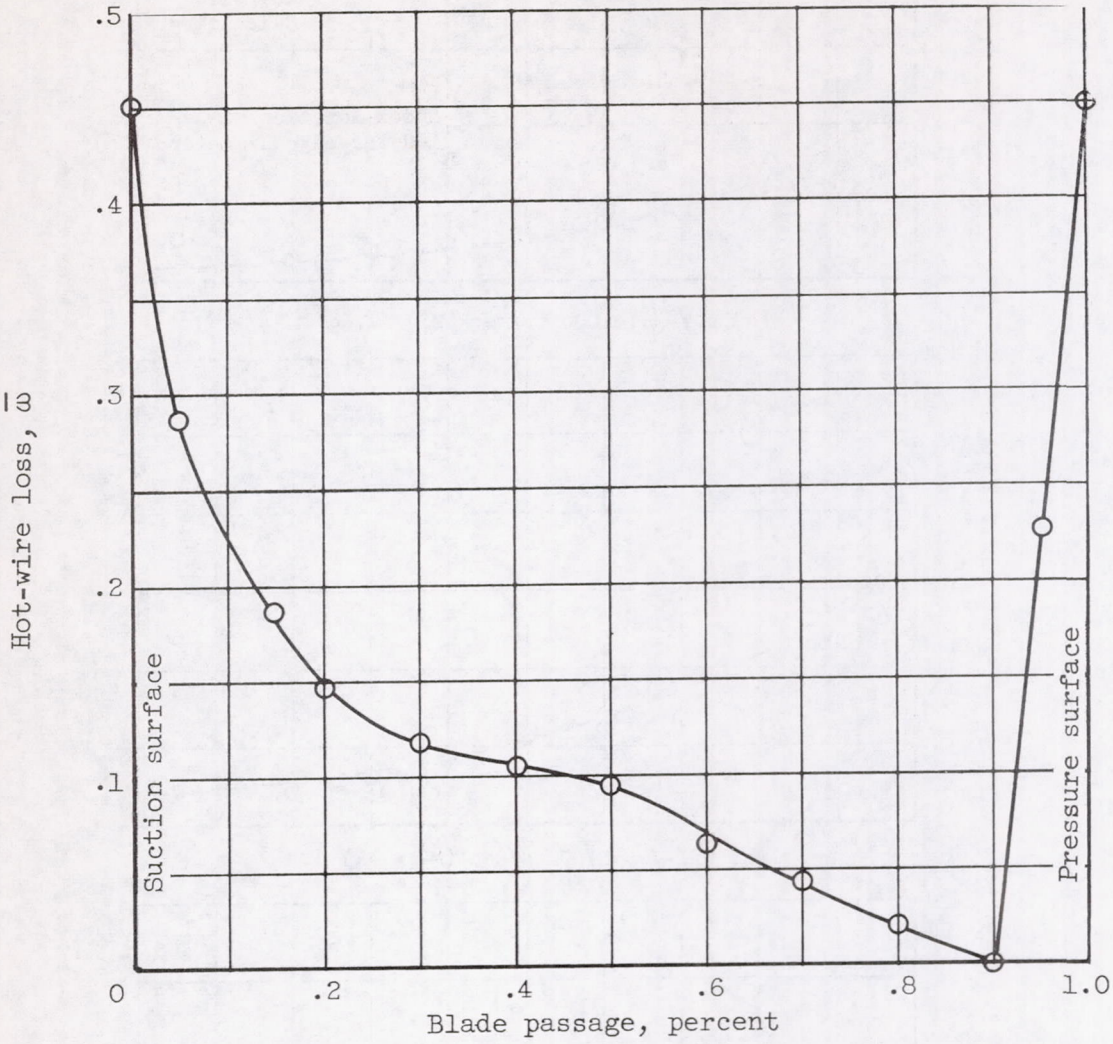
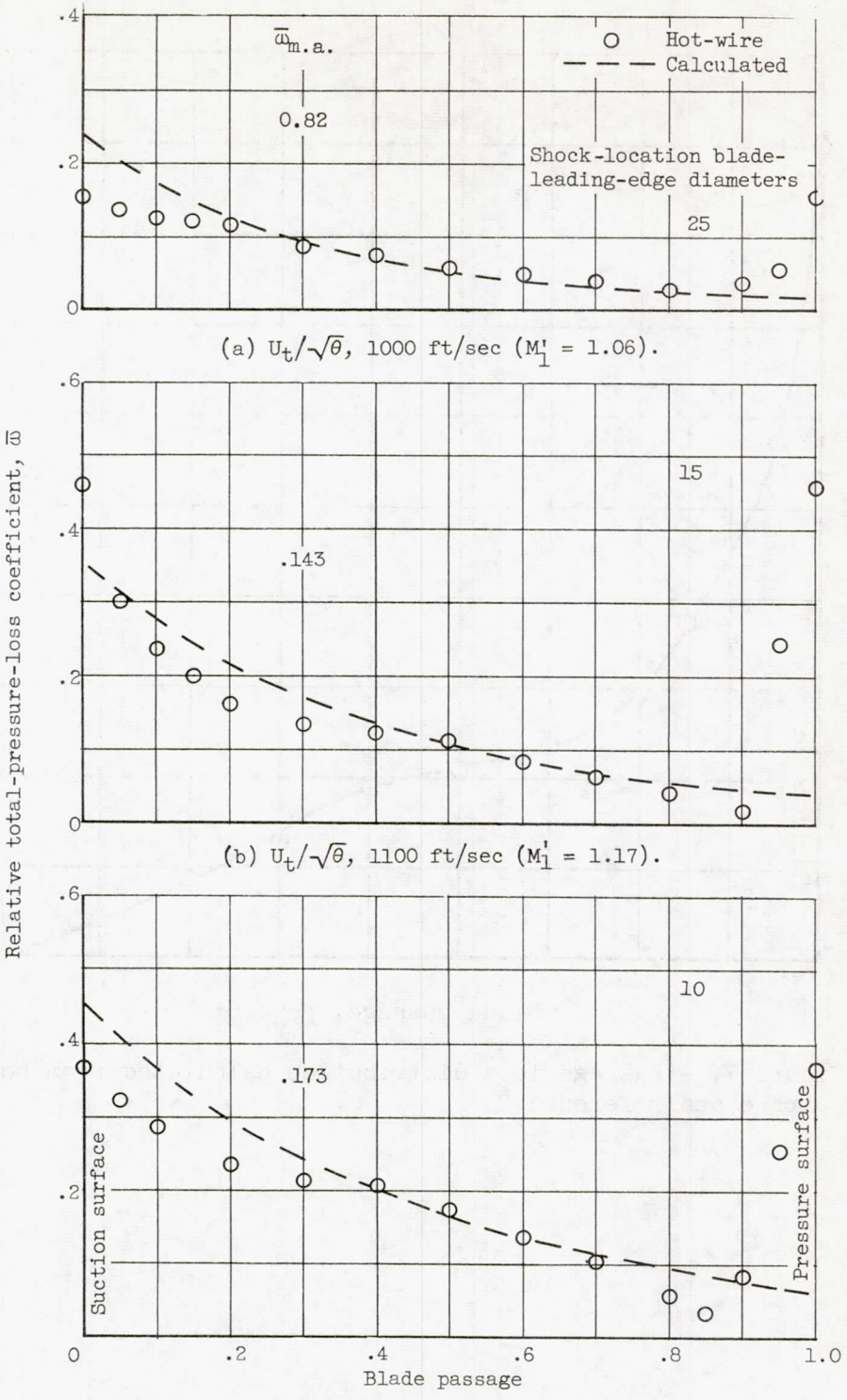


Figure 7. - Passage loss distribution calculated from hot-wire trace and reference 2.

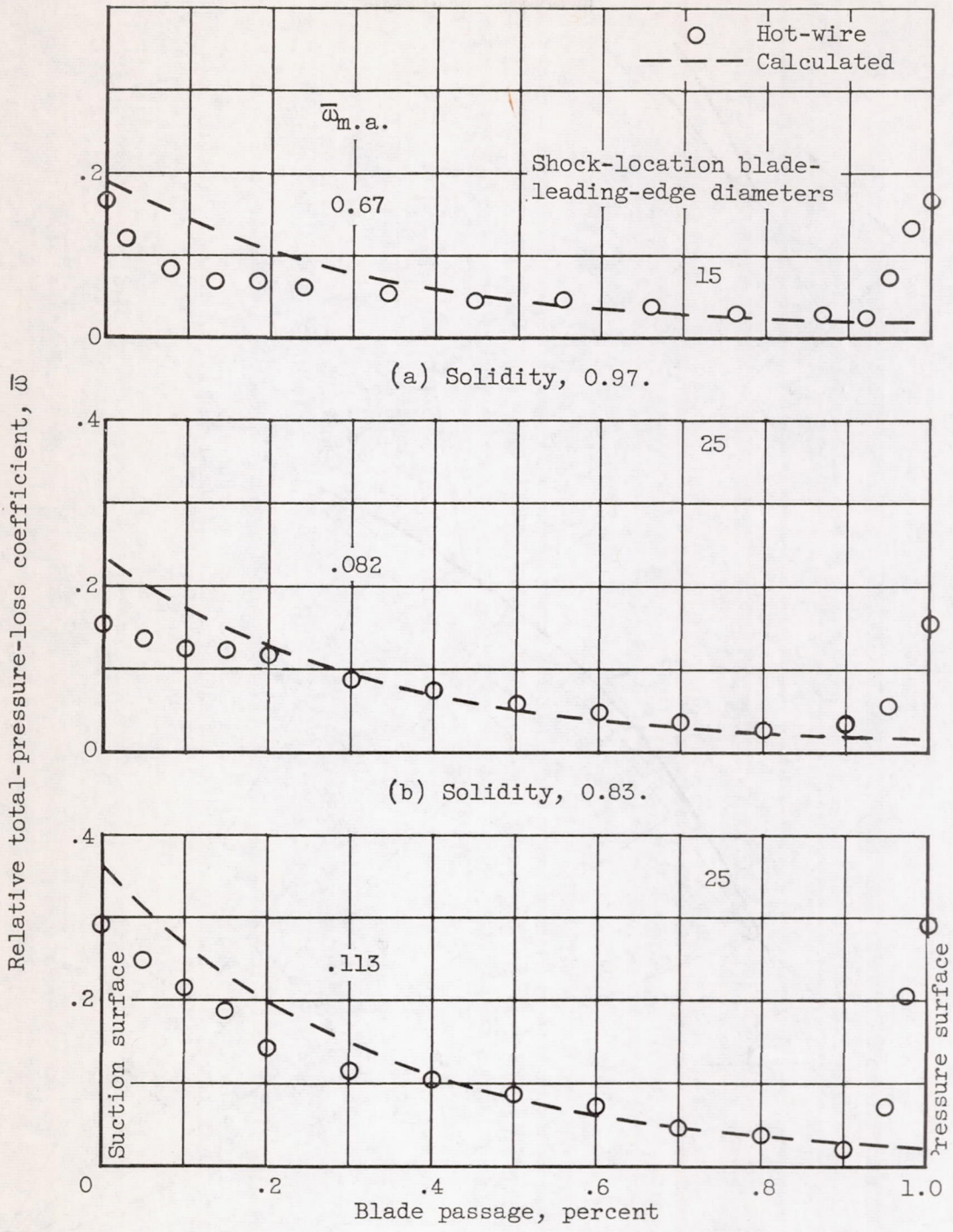


(a) $U_t/\sqrt{\theta}$, 1000 ft/sec (M_1' = 1.06).

(b) $U_t/\sqrt{\theta}$, 1100 ft/sec (M_1' = 1.17).

(c) $U_t/\sqrt{\theta}$, 1200 ft/sec (M_1' = 1.26).

Figure 8. - Hot-wire loss and computed shock-loss distribution across a blade passage for the 0.83-solidity compressor rotor.



(a) Solidity, 0.97.

(b) Solidity, 0.83.

(c) Solidity, 0.69.

Figure 9. - Hot-wire loss and computed shock-loss distribution across a blade passage for three compressor rotors at a corrected tip speed of 1000 feet per second.

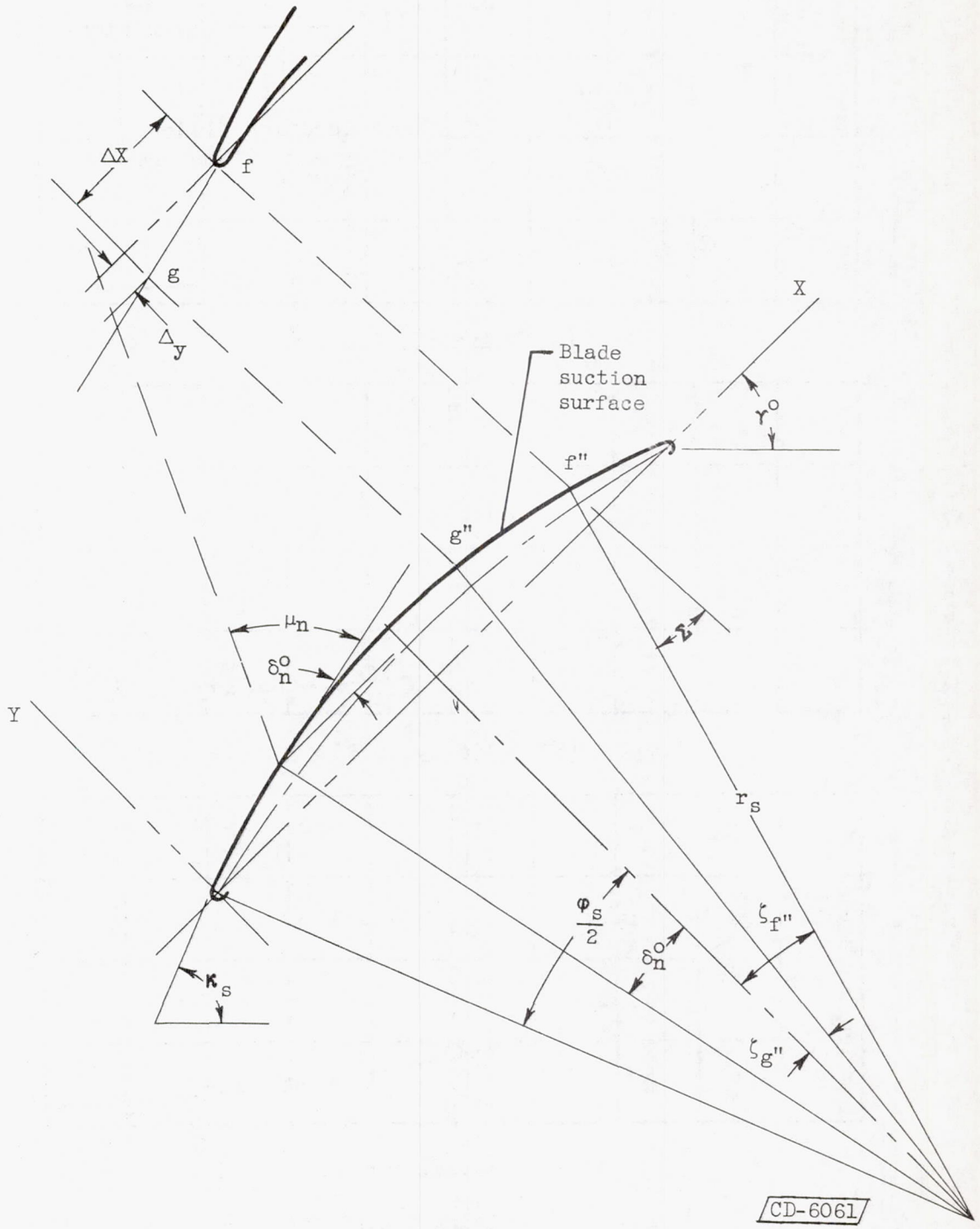


Figure 10. - Circular-arc blade geometry and shock location.